

Reinforcement Learning Based Quantum Circuit Optimization via ZX-Calculus

Jordi Riu^{1,2}, Jan Nogué¹, Gerard Vilaplana¹, Artur Garcia-Saez^{1,3}, and Marta P. Estarellas¹

¹Qilimanjaro Quantum Tech, Carrer dels Comtes de Bell-Lloc, 161, 08014 Barcelona, Spain

²Universitat Politècnica de Catalunya, Carrer de Jordi Girona, 3, 08034 Barcelona, Spain

³Barcelona Supercomputing Center, Plaça Eusebi Güell, 1-3, 08034 Barcelona, Spain

We propose a novel Reinforcement Learning (RL) method for optimizing quantum circuits using graph-theoretic simplification rules of ZX-diagrams. The agent, trained using the Proximal Policy Optimization (PPO) algorithm, employs Graph Neural Networks to approximate the policy and value functions. We demonstrate the capacity of our approach by comparing it against the best performing ZX-Calculus-based algorithm for the problem in hand. After training on small Clifford+T circuits of 5-qubits and few tenths of gates, the agent consistently improves the state-of-the-art for this type of circuits, for at least up to 80-qubit and 2100 gates, whilst remaining competitive in terms of computational performance. Additionally, we illustrate its versatility by targeting both total and two-qubit gate count reduction, conveying the potential of tailoring its reward function to the specific characteristics of each hardware backend. Our approach is ready to be used as a valuable tool for the implementation of quantum algorithms in the near-term intermediate-scale range (NISQ).

1 Introduction

Quantum computation is a promising paradigm that exploits the principles of quantum mechanics to perform tasks that are intractable for classical computers. However, current quantum devices face significant challenges, such as the presence of noise and decoherence in the physical sys-

tems that implement quantum circuits [1]. These challenges limit the scalability and the reliability of quantum computation, and pose a major obstacle for achieving quantum advantage over classical computation. Therefore, it is essential to design and optimize quantum circuits in a way that minimizes the number of gates and the resources required, while preserving the functionality and the fidelity of the computation [2].

One of the common approaches for optimizing quantum circuits is to apply algebraic identities to perform gate permutations and gate cancellations in the original circuit [3, 4]. Using reinforcement learning (RL) [5] in combination with this approach is currently being explored with promising results [6, 7]. However, in the previous context, the action space for the RL agent grows quickly, as there are several types of gate identities that need to be identified and each of those may involve multiple gates. This makes it harder for reinforcement learning agents to explore and exploit the optimal actions, as they have to deal with a large and diverse set of possible gate permutations and cancellations.

To overcome these limitations, we instead use ZX-Calculus [8], a graphical language to reason about quantum computation, as our framework for quantum circuit optimization. Using ZX-Calculus for quantum circuit optimization has the advantage of requiring a smaller and simpler action space, as there are fewer types of rules that can be applied to ZX-diagrams, with each rule being applicable to tensors of any dimension. ZX rules describe graphical ways to operate between its basic elements, spiders and wires, while preserving the semantics of the computation. Moreover, any ZX-Calculus rule can be described with at most two of these spiders.

In this work, we incorporate RL and, more specif-

Jordi Riu: jordi.riu@qilimanjaro.tech

Jan Nogué: jan.nogue@qilimanjaro.tech

arXiv:2312.11597v3 [quant-ph] 4 Jun 2024

ically, the Proximal Policy Optimization algorithm (PPO) [9] to guide the optimization of quantum circuits through the ZX formalism. We define a reward function that reflects the quality of the circuit optimization and explore the space of possible transformations using the ZX-Calculus rules. This paper is the result of our previous exploratory work [10], where a similar approach was applied to optimize quantum circuits with Clifford gates, which are a subset of quantum gates that can be efficiently simulated on classical computers [11, 12]. In [10], convolutional neural networks were used to learn the ZX-Calculus rewrite rules, and the method was shown to improve the existing ZX-Calculus based optimization algorithms implemented in the PyZX [13] package for small circuits. However, some limitations concerning the use of convolutional neural networks were identified, such as the difficulty of handling variable-sized inputs and outputs, heavily limiting the scalability of the approach. In this work, we improve the approach by using graph neural networks [14] instead of convolutional neural networks, as they are better suited to capture the features of large-dimensional graph-like structures such as ZX-diagrams.

The rest of the article is structured as follows: Section 2 covers the state of the art of circuit optimization with ZX-Calculus. Section 3 presents the specifics of our ZX-RL optimization method. Section 4 reports the results of applying our method to non-Clifford circuits and evaluates them against other ZX-based and Gate-based algorithms. Finally, Section 5 summarizes the conclusions and the potential future work.

2 Quantum Circuit Optimization via ZX-Calculus: State of the Art

2.1 General Overview

A ZX-diagram is a graphical representation of a linear map between qubits by means of an undirected graph [15, 16]. The basic elements of a ZX-diagram are spiders (nodes) and wires (edges). Spiders can be of two types: Z and X, and they can be interpreted as tensors composed of Pauli-Z and Pauli-X eigenstates, respectively. Using the graphical notation for ZX-Calculus they are

represented as

$$\begin{aligned}
 \text{Z-spider}(\alpha) &::= |0 \dots 0\rangle \langle 0 \dots 0| + e^{i\alpha} |1 \dots 1\rangle \langle 1 \dots 1|, \\
 \text{X-spider}(\alpha) &::= |+\dots+\rangle \langle +\dots+| + e^{i\alpha} |-\dots-\rangle \langle -\dots-|,
 \end{aligned}
 \tag{1}$$

where m and n are the number of inputs and outputs of the spider, respectively, and α is a phase between 0 and 2π . The wires in the diagram can also be of two types, typically referred to as Simple and Hadamard wires¹. A ZX-diagram can be simplified by applying a set of rules that preserve the underlying tensor representation of the diagram (see a summary of the rules in Figure 1). ZX-diagrams have a more open structure than quantum circuits, and their transformation rules are applicable regardless of the dimension of the spiders (tensors) involved. Notably, these rules can and give rise to transformations that can not always be described by single or two-qubit identities. A particularly relevant representation is expressing a ZX-diagram in its *graph-like* form [17]. The graph-like form of a ZX-diagram is such that

1. All spiders are Z-spiders (green spiders).
2. All connections between spiders are Hadamard wires (blue wires).
3. There are no parallel Hadamard edges or self-loops.
4. Every input and output is connected to at least one spider, and every spider is connected to at most one input or output.

This transformation can always be achieved by iteratively applying the spider fusion and Hadamard rules, and additional rules derived in [17]. Once in its graph-like form, the diagram can be operated with a different set of rules, based on graph-theoretic simplifications, that are described in Section 2.2.

Quantum circuit optimization via ZX-Calculus involves the following steps: First, one should transform the quantum circuit into its equivalent ZX-diagram. This diagram is then converted into its *graph-like* form and simplified using graph-theoretic rules. After the simplification process is finished, one needs to transform the diagram

¹A Hadamard wire is a simple wire with a Hadamard gate applied to it, and it is painted in blue.

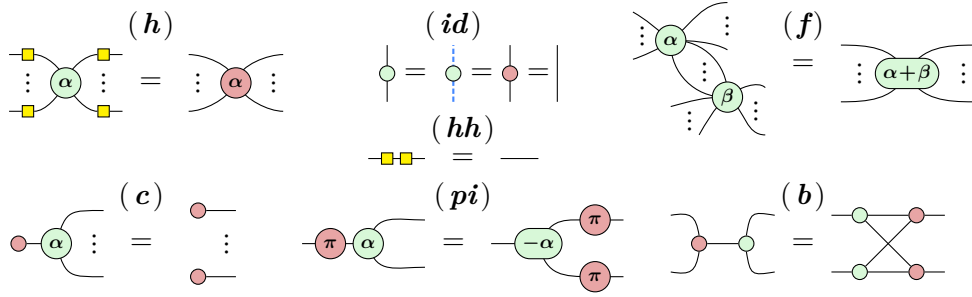
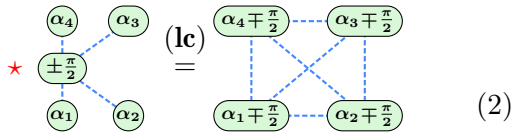


Figure 1: A summary of the ZX-Calculus. Note that ‘...’ reads as any integer $n \in \mathbb{Z}$. The letters stand respectively for **(h)**adamard, **(id)**entity, **(hh)**-cancellation, spider-**(f)**usion, **(c)**opy, **(pi)**-commute and **(b)**ialgebra. These rules hold for green or red spiders, for any orientation of the diagram and up to non-zero scalars.

back into an equivalent quantum circuit. This last step can be very inefficient or even unfeasible in some cases [18]. Even in the cases where this step is efficient, it can output circuits that are more computationally-expensive than the initial ones. This will be further discussed in Section 2.5. Although some heuristic rules have been suggested [19, 20], there is no known optimal strategy to tell which sequence of rule applications will yield the maximally optimized underlying circuit. The main focus of this paper is to improve the rule selection process using RL, rather than discovering new rules to simplify the diagram.

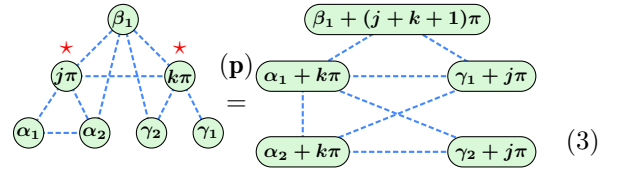
2.2 Graph-theoretic rules

Local complementation (Eq.2) and pivoting (Eq.3)[17] are the two essential rules that are used for the simplification of graph-like diagrams, and are inspired in their counterparts from graph theory [21, 22]. Local complementation can be applied to spiders whose phase is $\pm\pi/2$ (or proper Clifford spiders, marked with \star),



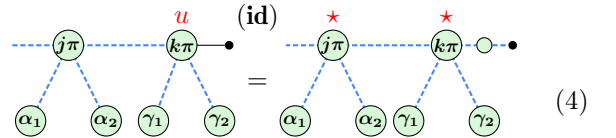
provided that they are connected by Hadamard wires to all of their neighbours and that they are all green spiders. This transformation, removes the target spider from the diagram and modifies the connectivity of its neighbourhood by complementing it, i.e., two neighbours that were connected become disconnected, and two neighbours that were disconnected become connected. Additionally, the phases of the neighbours are updated by subtracting the phase of the removed spider. On the other hand, pivoting **(p)** can be applied

to a pair of interior connected spiders with phase equal to 0 or π (Pauli spiders) that are only connected to green spiders through blue wires

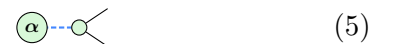


This rule transforms the graph by removing the pair of spiders at the cost of performing local complementation on three subsets: the unique neighbourhood of the first spider $\{\alpha_1, \alpha_2\}$, the unique neighbourhood of the second spider $\{\gamma_1, \gamma_2\}$ and the common neighbourhood of both spiders $\{\beta_1\}$. In short, any edge connecting nodes from different subsets will disappear, and vice versa. The phases of the remaining nodes are also updated as described in the aforementioned equation.

The pivoting rule can also be applied to remove a spider (u) that is adjacent to a boundary spider, i.e., an input or output of the circuit (**p1**). To do so, one needs to apply the **(id)** rule to transform the black wire as



After this transformation, pivoting can be applied to remove the marked vertices. Further rules have been developed to simplify non-Clifford spiders (i.e., spiders with a phase that is not a multiple of $\frac{\pi}{2}$), allowing to address the optimization of universal quantum circuits via phase gadgets: a α -phase spider connected by a Hadamard edge to a phase less spider.



Phase gadgets enable the modification of both **(p)** and **(p1)** to work with non-Clifford spiders, at the expense of introducing a phase gadget after the application of each rule (Eq. (6) **(p2)**, Eq. (7) **(p3)** respectively).

(p2)

$$\begin{array}{c} \beta_1 \\ \star \quad \star \\ \alpha_1 \quad \alpha_2 \quad \gamma_1 \quad \gamma_2 \\ \text{---} \quad \text{---} \quad \text{---} \quad \text{---} \end{array} = \begin{array}{c} \beta_1 + (j+k+1)\pi \\ \alpha_1 \quad \alpha_2 \quad \gamma_1 + j\pi \quad \gamma_2 + j\pi \\ \text{---} \quad \text{---} \quad \text{---} \quad \text{---} \\ (-1)^j \sigma \end{array} \quad (6)$$

(f, id)

$$\begin{array}{c} k\pi \\ \sigma \\ \alpha_1 \quad \alpha_2 \quad \gamma_1 \quad \gamma_2 \\ \text{---} \quad \text{---} \quad \text{---} \quad \text{---} \end{array} = \begin{array}{c} k\pi \\ \sigma \\ \alpha_1 \quad \alpha_2 \quad \gamma_1 \quad \gamma_2 \\ \text{---} \quad \text{---} \quad \text{---} \quad \text{---} \end{array} \quad (7)$$

Additionally, phase gadgets can be simplified with two rules: **(if)** removes a phase gadget with a single leg and **(gf)** fuses two phase gadgets when they are connected to the same set of neighbours:

(if)

$$\begin{array}{c} \beta \\ \alpha \\ \text{---} \end{array} = \begin{array}{c} \alpha + \beta \end{array}$$

(gf)

$$\begin{array}{c} \alpha \quad \alpha' \\ \sigma \quad \sigma' \\ \beta \quad \beta' \\ \text{---} \quad \text{---} \end{array} = \begin{array}{c} \alpha \quad \alpha' \\ \sigma + \sigma' \\ \beta \quad \beta' \\ \text{---} \quad \text{---} \end{array} \quad (8)$$

2.3 Circuit Extraction

Current circuit extraction algorithms make use of a necessary property for a deterministic graph state called *generalised flow* or *gflow* [23] from the Measurement Based Quantum Computing (MBQC) model [24]. Graph-like diagrams can be interpreted as an extension of a MBQC graph state where the phases of the spiders represent measurements on the XY, XZ or YZ of the Bloch sphere. In such diagrams, spiders are in the XY plane and phase gadgets are in the YZ plane. In [25] the authors developed a polynomial time extraction algorithm to extract a circuit from a graph state containing measurements in all three planes. Particularly, the algorithm extracts α -spiders into a $R_Z(\alpha)$ gate and the Hadamard wires into either a Hadamard, Controlled-Z (CZ), or a combination of CNOT gates which is generally contingent on the connectivity of the graph. Furthermore, spiders in the XZ and the YZ plane need to be converted into spiders in the XY plane, which results in an addition of Hadamard wires during the extraction process. The existence of

gflow in a transformed diagram is guaranteed if the initial diagram has gflow, as it is the case for quantum circuits, and the rules applied preserve it. Its exact calculation is not required for circuit extraction, the knowledge that one exists suffices. It should also be noted that the circuit extraction process can induce the addition of gates that can be trivially simplified afterwards with a gate-based optimizer. In this work, the extraction algorithm is treated as a black box that cannot be optimized, and we limit our action space to rules that satisfy the gflow condition, such as the ones described in Section 2.2.

2.4 Simplification algorithms

In this section, we review three simplification algorithms based on ZX-Calculus, each targeting the reduction of different types of spiders or gates in the resulting circuit. These algorithms will be used to benchmark our approach and, to the best of our knowledge, represent the state of the art of the field.

2.4.1 Simplification of interior Clifford spiders

In [17] the first algorithm for quantum circuit optimization using ZX-Calculus was introduced. Starting from the diagram in its graph-like form, the algorithm is applied as follows:

1. Apply **(lc)** to remove all interior spiders with phase $\pm\pi/2$.
2. Apply **(p, p1)** to remove adjacent pairs of spiders with phase 0 or π whether they are interior or one of them is not.
3. Apply **(p2, p3)** to remove adjacent pairs of Clifford and non-Clifford spiders (with both interior or one of them boundary).
4. Apply **(gf)** to further reduce non-Clifford spiders.

This sequence of rules is followed iteratively until there are no transformations available and the process terminates. In this regard, it is crucial to understand the trade-off between removing a spider and altering the connectivity of the diagram, as this may imply a reduction in the total number of gates but also increase the number of two-qubit gates (Figure 2b). This algorithm is implemented under the name of `full_reduce` in the library PyZX.

2.4.2 Simplification of non-Clifford spiders

In [26], the authors introduced an algorithm to optimize the T-count, i.e., the number of T gates required to implement the quantum circuit, using ZX-Calculus. The authors first parameterize the original circuit, $C[\alpha_1, \dots, \alpha_n]$, where $\alpha_1, \dots, \alpha_n$ are variables representing the phases of the spiders. The phases are stored in a table $\tau : \{1, \dots, n\} \rightarrow \mathbb{R}$ such that the original circuit can always be retrieved with $C[\tau]$. The algorithm then proceeds to run the `full_reduce` on $C[\tau]$ and *symbolically* tracks the phases after two variables are added together. Specifically, after the application of the rules (**if**) and (**gf**), depending on the sign difference between the affected variables, i, j , the table τ can be updated as: $\tau'(i) := \tau(i) \pm \tau(j)$, $\tau'(j) := 0$ and $\tau'(k) := \tau(k) \forall k \notin \{i, j\}$, generating an equivalent ZX-diagram. After the termination of the `full_reduce`, the final circuit is obtained with $C[\tau']$, which will possibly contain fewer non-Clifford gates. This technique is denominated *phase teleportation*. By construction, the phase teleportation algorithm results in the same T-count as the `full_reduce`. However, phase teleportation does not change the original structure of the circuit, and in particular, the number or location of the two qubit gates. Therefore, employing phase teleportation as a initial processing in a compound simplification algorithm is rather convenient, as the further simplifications could potentially perform better since, in general, there will be less 'blockage' in the form of non-Clifford gates. This algorithm is implemented under the name of `teleport_reduce` in the library PyZX.

2.4.3 Simplification of two-qubit gates

As mentioned, it is extremely complicated to predict the exact number of two-qubit gates that will be obtained after the circuit extraction of ZX-diagrams preserving gflow. However, in [20] the authors try to do so using heuristics based on the number of Hadamard wires obtained after a rule application, precisely to avoid a highly connected ZX-diagram. To apply (**lc**) and (**p**) to spiders with arbitrary phase, the rules (**f**, **id**) are introduced, similar to what is done in (**p2**). They find that applying (**lc**) and (**p**) to general spiders introduces spiders in the XZ and YZ plane, which add a significant amount of Hadamard wires in the circuit extraction that can not be optimized

with the heuristics used during the algorithm. To solve this issue, they also explore the use of the neighbour unfusion rule (**nu**) (with $|m| = 1$)

$$\left. \begin{array}{c} \vdots \\ \circlearrowleft \alpha \\ \vdots \end{array} \right\} m = \left. \begin{array}{c} \text{(nu)} \\ \vdots \\ \circlearrowleft \alpha - \beta \text{---} \circ \text{---} \beta \\ \vdots \end{array} \right\} m \quad (9)$$

which turns out very effective in the reduction of two qubit gates but that does not always preserve gflow. The authors present a greedy algorithm, guided with the heuristics, that selects (**lc**) and (**p**) until termination, which we denominated as **gflow-heur**. Summarizing, preserving gflow allows deviating from the rigid circuit structure and thus enhances exploration of graph-states where an effective optimization can be found. However, using this formulation, it is unclear how to predict the resulting amount of two-qubits gates without performing circuit extraction.

With this goal in mind, in [19] the authors introduce an optimization algorithm based on rules preserving *causal flow* or *cflow* which is a stricter condition than gflow, though not necessary, for a deterministic MBQC graph-state [27]. Even though only (**if**) is known to preserve cflow, there exists a computationally feasible algorithm introduced in [28] (which scales as $\mathcal{O}(|I||V|)$ compared to the gflow calculation algorithm that scales as $\mathcal{O}(|V|^4)$, with I, V the Inputs and Vertices set) that allows the authors to compute cflow after a rule application, thus ensuring the cflow preservation throughout the simplification algorithm. The advantage of preserving cflow is precisely that there exists a direct equivalence between a graph-state and its underlying circuit, which results in a direct way of computing the two-qubit gate count, at the cost of deviating less from the rigid circuit structure and therefore leaving less room for exploration of more complex ZX-diagrams. The authors present a greedy algorithm that selects (**if**, **lc**, **p**) alone or combined with (**nu**) with up to $|m| = 2$ (to apply to general spiders) that prioritizes termination, which we denominate as **cflow-heur**.

2.5 General remarks and tests

To illustrate the performance of the aforementioned optimization algorithms, we conducted a test on random Clifford+T circuits of 10 qubits,

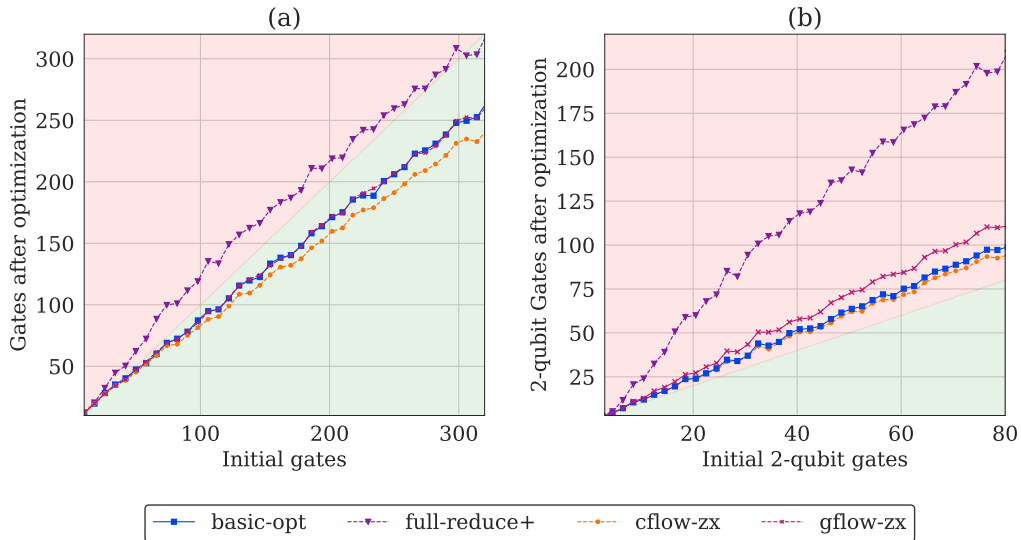


Figure 2: Total amount of gates after the optimization of quantum circuits using the `basic-optimization` algorithm (`basic-opt`, blue), the `full_reduce` algorithm (purple), the `cflow` preserving algorithm (`cflow-zx`, orange) and the `gflow` preserving algorithm (`gflow-zx`, magenta). Tests conducted on 10-qubit Clifford+T, with an increasing number of initial gates. Shaded regions in red indicate instances of unsuccessful compression, while those shaded in green denote successful compression. (a) Total Gate Count (b) Two-qubit Gate Count.

with uniform probability of inclusion of each type of gate (S,T,CNOT,HAD). The first algorithm depicted is implemented under the name of `basic_optimization` in the PyZX library (`basic-opt` in the plot, illustrated in blue). It is a peephole optimizer that runs the circuit back-and-forth applying SWAP and gate cancellation identities until no further simplifications can be made. Note that since the extract circuit procedure usually adds gates combinations that can be trivially cancelled, this algorithm is a perfect fit as a post-processing step after the optimization. The second algorithm compared is the `full_reduce` (illustrated in purple) with the `basic_optimization` as a post-processing step. As mentioned, the application of all available rules until termination yields suboptimal results, significantly increasing the quantity of two-qubit gates for relatively shallow circuits (Figure 2b), and being outperformed by the simple gate-based optimizer (Figure 2a). The third and fourth algorithms are based on the `cflow-heur` and `gflow-heur` heuristics explained in Section 2.4.3 and are denoted as `cflow-zx` (in orange) and `gflow-zx` (in magenta) respectively. Both algorithms include the `basic_optimization` plus the `teleport_reduce` as a pre-processing step to simplify trivial identities and reduce the T-count. Additionally, the `basic_optimization`

is included after circuit extraction as a post-processing step. The `cflow-zx` algorithm manages to outperform the previous algorithms by reducing both the number of single and two-qubit gates. Considering the existing results presented for the previous algorithms and the ones we obtained for the specific type of circuits under study, we choose the `cflow-zx` algorithm to benchmark against our approach because, to the best of our knowledge, there are no algorithms based on the preservation of `gflow` that are competitive both in quality and computational performance for non-Clifford circuits.

3 RL-ZX Based Quantum Circuit Optimization

3.1 Proximal Policy Optimization

RL is a machine learning paradigm in which an agent learns, through trial and error, to perform a task on an environment. A training loop in RL follows a simple structure: The agent receives an observation s of the current state of the environment and picks its next action a upon a set of available ones using the experience gathered from previous attempts. Afterwards, the environment

returns both a reward for the performed action and a new observation that can be used to update the agent strategy.

There are a myriad of RL algorithms that have found success in applications for many diverse fields. In this work, we use the *Proximal Policy Optimization* algorithm (PPO), which has a positive track record in similar circuit optimization settings. The PPO algorithm is a policy-gradient method which relies on the optimization of the parameters of a policy function $\pi(a|s)$. This function returns the optimal action to be performed given an observation. Additionally, the agent guides its learning process by interpolating a value function that estimates the expected value of the returns for a given state, $V(s)$. Both

$\pi(a|s)$ and $V(s)$ functions are typically approximated using Deep Neural Networks (DNNs). The DNN used for approximating the policy function is often referred to as the *actor*, as it determines the optimal action in a given state. On the other hand, the DNN used for approximating the value function is known as the *critic*, as it evaluates the expected returns for a given state. This actor-critic architecture is a common approach in RL algorithms. During the training phase, the optimization of the parameters for both networks is done simultaneously by minimizing the loss function

$$L^{PPO}(\theta) = L^{Actor}(\theta) + c_1 L^{Critic}(\theta) - c_2 L^{Entropy}(\theta), \quad (10)$$

with $L^{Actor}(\theta)$, $L^{Critic}(\theta)$ and $L^{Entropy}(\theta)$ defined as

$$L^{Actor}(\theta) = \hat{E}_t \left[\max \left(-\frac{\pi_\theta(a_t|s_t)}{\pi_{\theta_{old}}(a_t|s_t)} A_t, -\text{clip} \left(\frac{\pi_\theta(a_t|s_t)}{\pi_{\theta_{old}}(a_t|s_t)}, 1 - \epsilon, 1 + \epsilon \right) A_t \right) \right], \quad (11)$$

$$L^{Critic}(\theta) = \frac{1}{2} \hat{E}_t \left[\max \left((V(s_t) - V_t^{\text{target}})^2, (V_{\text{clip}}(s_t) - V_t^{\text{target}})^2 \right) \right], \quad (12)$$

$$L^{Entropy}(\theta) = -\hat{E}_t \left[\sum_{i=1}^n \pi_\theta(a_i|s_t) \log(\pi_\theta(a_i|s_t)) \right], \quad (13)$$

The policy loss, $L^{Actor}(\theta)$ in Eq.11, is computed as the product of the ratio of probability change between policies and the Generalized Advantage Estimator(A_t)[29] which, in simple words, measures how much better an action is compared to the average action at a given state. Hence, this term decreases if the new policy increases the probability of selecting actions with higher returns with respect to the previous one, and likewise, it reduces the probability of selecting non-beneficial actions. The critic loss, $L^{Critic}(\theta)$ (Eq. 12), essentially corresponds to the mean-squared error between the critic network’s prediction and the actual return obtained by the agent. Hence, it is a measure of how well the critic can estimate the expected return given a state. Both terms can be slightly modified to include clipping restrictions that limit the amount of change in each function at each step, so as to achieve a more stable training.

The last term in the loss function, $L^{Entropy}(\theta)$ in Eq.13, is included in order to balance explo-

ration and exploitation during training. Exploration refers to the process of experimenting with novel actions that may potentially yield superior outcomes in subsequent stages. Conversely, exploitation involves adhering to the most advantageous known actions to optimize immediate rewards. An effective reinforcement learning agent should have sufficient exploration capacity in order to uncover new and improved actions, while also exploiting adequately to avoid wasting time and resources on the optimization of networks for the interpolation of suboptimal actions. In PPO, the entropy term is equivalent to the entropy of the log-probabilities produced by the actor network. Given that the entropy loss is subtracted in the total loss function, this term effectively guides the agent towards parameter configurations that increase the policy’s uncertainty.

The PPO algorithm is known for its stability, as it avoids drastic policy updates that could lead to *catastrophic forgetting*, i.e., an abrupt change in the network that destroys the knowledge gained

from previous experiences. However, perhaps its most significant advantage is its sample efficiency, as it allows for the parallelization of the sample generation process, which means that multiple instances can be run simultaneously. This feature significantly speeds up the learning process. For our particular task in hand, this proves to be very beneficial as it allows the agent to gain experience from many different circuit configurations, allowing for better generalization capabilities.

3.2 Graph Neural Networks

Graph Neural Networks (GNNs) are a type of artificial neural networks that are particularly well suited to work with data that can be represented as graphs, as it is the case for ZX-diagrams. These type of networks typically involve *message passing* layers that propagate the information of each node of the network to its nearest neighbours, i.e., the nodes that are connected to it. Hence, by iteratively adding several of these layers, the network is capable to capture long distance correlations in the data.

There are numerous variants of Graph Neural Networks (GNNs) in the existing literature, each employing a unique method to integrate the information received from a node’s neighbours to update its current state. In this study, we utilize Graph Attention Networks (GATs), specifically GATv2 layers [30, 31]. These networks deviate from simpler GNNs by executing a weighted aggregation of information. The weights for this aggregation are computed using an attention layer in the calculation process. This allows the network to identify the significant neighbours of a node, namely those that contribute most significantly to the learning process. To elaborate further, let \mathbf{x}_i^t denote the input features to the GATv2 message passing layer, and let $\mathcal{N}(i)$ represent the set of neighbouring nodes. The output features \mathbf{x}_i^{t+1} are then computed as

$$\mathbf{x}_i^{t+1} = \alpha_{i,i} \Theta_s \mathbf{x}_i^t + \sum_{j \in \mathcal{N}(i)} \alpha_{i,j} \Theta_t \mathbf{x}_j^t, \quad (14)$$

where Θ_s and Θ_t are the learnable parameters to be optimized, and $\alpha_{i,j}$ represents the attention coefficient between node i and node j . In its turn,

these attention coefficients are obtained as:

$$\alpha_{i,j} = \frac{\exp(\mathbf{a}^\top \mathcal{G}(\Theta_s \mathbf{x}_i + \Theta_t \mathbf{x}_j + \Theta_e \mathbf{e}_{i,j}))}{\sum_{k \in \mathcal{N}(i) \cup \{i\}} \exp(\mathbf{a}^\top \mathcal{G}(\Theta_s \mathbf{x}_i + \Theta_t \mathbf{x}_k + \Theta_e \mathbf{e}_{i,k}))}, \quad (15)$$

with \mathbf{a} , Θ_s , Θ_t and Θ_e additional weights that can be learned through the minimization of the target loss function. $\mathbf{e}_{i,j}$ represent the features of the edge connecting nodes i and j in the graph. Note that, unlike for the node features, these remain unchanged during the calculation. The \mathcal{G} function corresponds to the LeakyReLU activation function. Finally, note that a Softmax normalization is used so that the sum of attention coefficients for each node always adds up to 1.

3.3 RL Agent: Structure and Learning Process

The schematic representation of the training process is depicted in Figure 3. Each training episode involves the generation of a random circuit, which is then transformed into a graph-like diagram. At each step, the agent selects an action from the available choices, based on the diagram’s state. After the action is applied, the circuit is extracted from the modified diagram, and rewards are allocated based on the total number of gates obtained. The training utilizes the PPO algorithm, with both $\pi(a|s)$ and $V(s)$ networks incorporating GATv2 layers. We apply both the `basic_optimization` and `teleport_reduce` algorithms before the agent starts acting on the circuit, which we laxly denominate as `gate-based`. The former removes trivial gate identities, reducing the workload of the agent. The latter reduces the amount of T gates in the circuit, which are hard to simplify with the action set at the agent’s disposal.

The action space is restricted to local complementation (`lc`), pivoting (`p`, `p1`, `p2`, `p3`), gadget fusion (`gf`) and identity (`id`) rules only, with an additional action that the agent can select to terminate the episode (`STOP`). A detailed analysis of the architecture and methodology is required to effectively incorporate neighbour unfusion, as it is not guaranteed to preserve the *gflow*.

3.3.1 Actor and Critic

The actor layer’s architecture comprises multiple *GATv2* layers. A layer configuration replicates the structure of the ZX-diagram, as depicted in

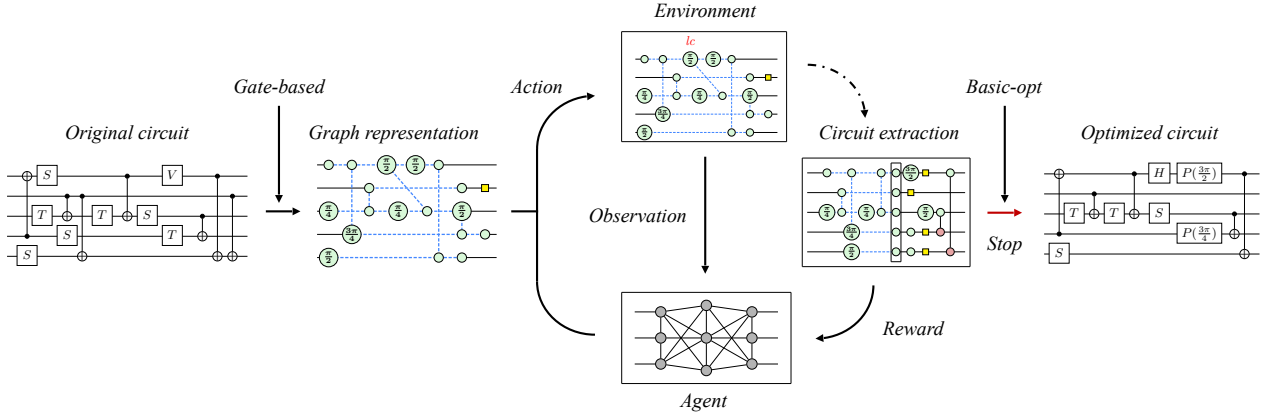


Figure 3: Overview of the r1-zx approach. From a random quantum circuit, the equivalent ZX-diagram in graph-like form is obtained. The agent uses its learned policy to choose between several graph transformations to be applied to the ZX-diagram (see Figure 4 for the details on the actor and the critic network structures). After the action is applied, the environment returns the resulting diagram to the agent as an observation, as well as its corresponding reward that is obtained after extracting the new circuit. The process is repeated until the agent decides to terminate the episode or no actions are available.

Figure 4. Each green spider in the diagram is associated with a corresponding node in the network. In addition, every feasible rule that can be applied, defined by its type and the nodes that explicitly characterize it, is incorporated as a node within the network. These action nodes are connected solely to the nodes that define them and to the *STOP* action node. The connectivity pattern of the nodes derived from the green spiders is identical to that in the ZX-diagram. The *STOP* action is only linked to the other action nodes in the graph. Upon completion of the message passing layers, the feature vector of each action node, denoted as x_a^t , undergoes a transformation via the Softmax activation function. This process computes the probability of selecting a particular action, represented by $\pi(a_i|s)$, which is defined as

$$\pi(a_i|s) = \frac{\exp(x_{a_i}^t)}{\sum_{a \in \mathcal{F}(s)} \exp(x_a^t)}, \quad (16)$$

Here, $\mathcal{F}(s)$ denotes the set of all feasible actions applicable to the current state s of the ZX-diagram. Initially, each node j in the policy network is described by a 16-dimensional feature vector x_j^{init} with the following attributes: eight binary flags indicating the phase of the node if any ($0, \pi/4, \pi/2, 3\pi/4, \pi, 5\pi/4, 3\pi/2$ or $7\pi/4$), three binary flags indicating whether the node represents an input, an output or a phase gadget, and 5 binary flags that identify whether the spider functions as a local complementation node, a pivoting node, a STOP node, an identity node or

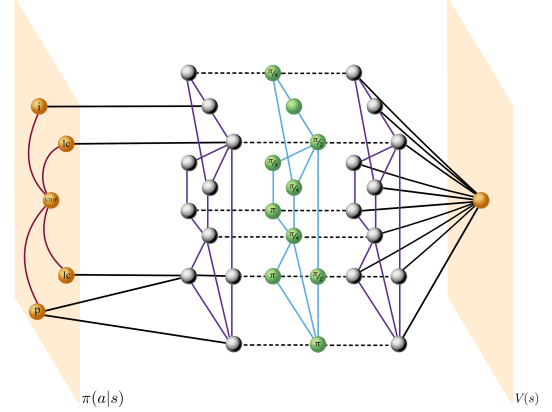


Figure 4: Schematic Overview of the Actor and Policy Networks: The policy network, denoted by $\pi(a|s)$, is visualized with each green spider from the diagram corresponding to a silver node, while the blue wires are depicted as purple connections. Action nodes are highlighted in orange, with connections to silver nodes and node STOP, which provide a complete description of the actions. The critic network shares a similar architecture; however, the orange node, representing the $V(s)$ output, is not part of the message passing layers. Instead, it is obtained after applying the global attention layer to the outputs of such layers. The self loops are not included for clarity.

a gadget fusion node. These features collectively provide a comprehensive representation of the node’s state within the network. For the critic network, only the first 11 features are included, as no action nodes are required. Additionally, each edge in the actor network is assigned a 6-dimensional *one-hot* vector that serves to distinguish the type of connection it represents, i.e., a wire in the ZX-diagram or a connection between a node in the diagram and an action node of each given type. The term one-hot refers to a vector where only one element is “hot” (set to 1) while all other elements are “cold” (set to 0). Additionally, we also include self loops to each node as per the original formulation of the GATv2 layers [31].

3.3.2 Reward Function

After each action, the agent receives a reward that is equal to the difference between the amount of gates before the action is applied to the graph-like diagram and after. This reward is normalized by an expected compression factor that depends on the number of qubits and the initial number of gates of the circuit. We train the agent on two differentiated rewards: the first targets the total number of gates, whilst the second only considers the number of two-qubit gates. As explained above, the circuit extraction procedure can be quite inefficient, not only substantially increasing the amount of two-qubit gates in the circuit but also including single-qubit gates that can trivially be simplified afterwards. This overhead leads the agent to discard actions that achieve non-trivial simplifications. For this reason, the `basic_optimization` algorithm is applied before calculating the reward given to the agent. This inclusion slows down the training process, but for testing purposes, circuit extraction can be used only at the end of the episode, if desired. Additionally, we include a single shot reward at the end of the episode proportional to the difference in gates achieved by the agent and the `cflow-zx` optimizer for the same circuit. We find that, without this reward, controlling the balance between exploration and exploitation with only the entropy parameter is extremely hard, and the agent tends to rapidly converge to a policy of not applying actions to the circuit.

4 Experiments and Results

Establishing an appropriate and representative benchmark for evaluating our `rl-zx` strategy presents a significant challenge. The complexity arises from the fact that the results obtained not only depend on the agent’s performance, but also on the rest of algorithms used in our workflow. These elements are treated as a black-box by the agent (i.e., the agent has no control nor information on its behaviour). This could lead to the conclusion that the agent’s performance is suboptimal, even in scenarios where it had no opportunity to have a meaningful impact on the process. To partially circumvent this issue, we keep the best circuits obtained by the agent at any point during the optimization, not just at the end of the episode. This has the drawback of requiring the extraction of the circuit after each step in the optimization, penalizing the computational performance of our approach as a trade-off. In some cases, for which the agent is incapable of making any useful actions, the output circuit is directly the one obtained after the `basic_optimization` and `teleport_reduce` algorithms are applied. However, this is a very unlikely occurrence, as we will see below.

In evaluating our methodology, three criteria are considered: the quality of the outcomes, computational efficiency and the capacity of the agent to generalize to larger instances. These criteria are assessed against the previously selected benchmark. Notably, the `cflow-zx` preserving algorithm uses a different action space and a different circuit extraction method, but it is the best existing ZX-based optimization algorithm. Regarding scalability, it is noteworthy that while a trained RL agent can swiftly optimize circuits, the training phase itself can be time-intensive. Consequently, it is crucial to determine whether agents trained on smaller circuits, which require shorter training periods, are capable of effectively generalizing to larger-scale instances.

All experiments are done for randomly generated Clifford+T circuits and considering the two targets of optimization described above, i.e., the total amount of gates or two-qubit gates only. For the former, we train the agent on circuits of 5 qubits and 60 gates with equal probability of inclusion for each gate type. On

Table 1: PPO hyperparameters used to train our agent

Parameter	Value
Num. steps	512
Num. environments	8
Learning rate (η)	2×10^{-4}
Num. epochs	8
Minibatch size	512
Discount (γ)	0.99
GAE parameter (λ)	0.95
VF coeff. c_1 (Eq.10)	0.5
Entropy coeff. c_2 (Eq.10)	0.01
Clipping parameter. ϵ	0.1

average, these circuits have depth $d \approx 20$. To study the capacity for the agent to generalize to larger circuits, we will both increase the number of qubits and the average depth of the randomized circuits. For the latter, the agent trains on circuits of 5 qubits and 70 gates, with increased probability of including CNOT gates to $\frac{1}{3}$, to compensate for the reduction of meaningful actions for this optimization target.

Both trainings are done in a single node with 8 CPUs and a single GPU and take ~ 16 hours. The agent and the environment are implemented using PyTorch [32] and Gym [33], respectively. For the agent, both the actor and critic contain 5 *GATv2* message-passing layers, with input/output channel dimension of 32. The critic network incorporates a global attention layer following the *GATv2* layers. The additional hyperparameters used during the training are detailed in Table 1.

4.1 Analysis of the Optimization Policy

We first focus on understanding the differences between the learnt optimization strategies for both experiments. To do so, we test the obtained agent policies on 1000 random circuits of increasing number of qubits (5, 10, 20, 40 and 80) and increasing average depth (d , $2d$, $3d$, $4d$). For clarity, the largest instances are generated for 80 qubit circuits of 2100 random gates (which result on an average depth of 80). The probabilities of inclusion of each gate remain unchanged with respect to the training phase.

When optimizing the total amount of gates in the circuit, the agent consistently increases

the amount of simplified gates across both circuit depth and number of qubits (Figure 5a). Naively, this signals that the agent is able to generalize correctly. On the other hand, the agent’s performance seems to be mostly dependent on circuit depth when trying to reduce the amount of two-qubit gates (Figure 5b). However, when comparing the amount of actions that the agent performs before reaching the optimal circuit in an episode, this number increases across both circuit depth and number of qubits for both policies, until reaching the maximum length allowed, which varies between 50 and 100 depending on circuit size (Figure 6). To understand the scaling disparity between the optimal episode length and the compression achieved for each objective, we analyse the reward obtained per rule type for both optimization objectives, and find that local complementation is not impactful when optimizing two-qubit gates. This is seen by plotting the histogram of the change in gates produced by each action for all episodes (which we don’t include for brevity). Hence, when targeting two-qubit gate reduction, the agent relies almost exclusively on pivotings, whilst local complementation can be interpreted as equivalent to a *PASS* action, that neither benefits nor penalizes the agent immediately, although it produces a change in connectivity that may result in additional pivotings appearing next. With this in mind, we plot the average number of actions of each type that are selected by the agent for both policies (Figure 7). We observe that whilst local complementation rules do appear to follow the same monotonic increase with both circuit size dimensions, the agent struggles to find beneficial pivotings to apply to the circuit as the number of qubits grows (Figure 7b), resulting in the performance disparity for both optimization objectives. This can be understood by the fact that pivotings affect the neighbourhood of two-spiders, leading to drastic changes of connectivity in the diagram after applied. This variance is dependent on the number of wires a spider can have, which is directly linked to the dimension of the Hilbert space (i.e. the number of qubits) when preserving gflow. Hence, modelling the effect of pivotings on the circuit extraction process becomes particularly difficult, specially considering that the former is treated as a black-box. One could try to include

new features into the observation given to the agent to partially circumvent this issue, such as the heuristics that are used in [20]. We leave this as future work. Nonetheless, our findings are in accordance with the general conception that managing two-qubit gates reduction is the major limiting factor for ZX optimizers based on the preservation of gflow due to the inefficient circuit extraction process.

4.2 Quality of the compression

We assess the quality of the results obtained by our approach by comparing it with the `cflow-zx` and the `gate-based` algorithms (the combination of `basic_optimization` and `teleport_reduce` algorithms) i.e. the agent takes no action in the circuit. As previously mentioned, we consider the best circuit seen during an episode as the output of the `r1-zx` agent. This is relevant when increasing the size of the tests, as any misstep by the agent rapidly increases the amount of gates in the circuit.

Firstly, we study the frequency with which all the competing optimizers achieve the best result. Again, tests involve one thousand episodes per circuit size. For the total gate reduction, our approach consistently outperforms the competition for circuits of up to sixteen times in qubits and four times in average depth with respect to the training amount (5 qubits and depth 20) (Figure 8a). When optimizing for the amount of two-qubit gates, the difference is even more significant, with the agent winning in above 80% of the cases (Figure 8b) for the largest circuits. This demonstrates the utility of the approach in the regime of circuits that are expected to allow for quantum advantage experiments. Somewhat counterintuitively, the agent is clearly beaten by the competition for 5-qubit circuits of large depth (Figure 8b for 3d and 4d). This may be a consequence of the fact that the agent learns a somewhat "risk-free" policy, due to the high variance of the effect of an action, that is able to generalize well. Another factor to take into account is the fact that with the current observation features and the message-function implemented by `GATv2` layers, the agent has no information in regard to "extensive" properties of the graph (for instance, total number of nodes or total number of edges). We have also briefly explored using graph convolutional layers and aggregating

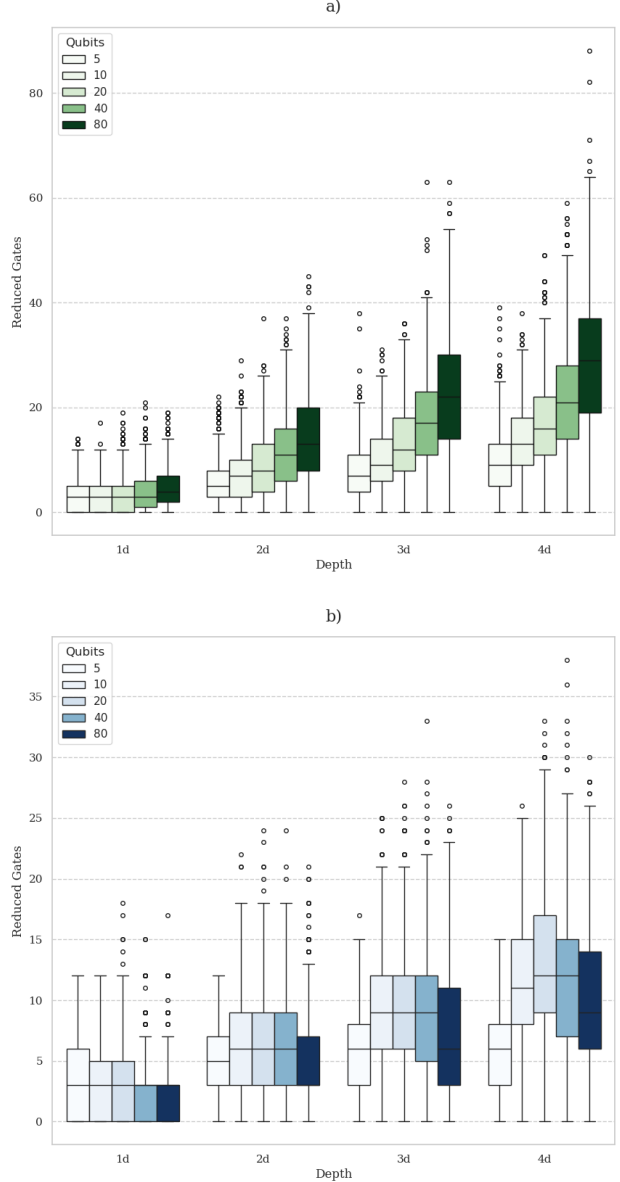


Figure 5: Box plot of the number of gates reduced by the `r1-zx` agent once trained. The initial value for comparison corresponds to the amount of gates after `basic_optimization` and `teleport_reduce` algorithms are applied to the circuit. Tests are performed for two-different tasks and across several circuit sizes, both in terms of number of qubits and average circuit depth. Statistics are drawn from one-thousand executions of random circuits for each circuit size and task. (a) Reduced single-qubit and two-qubit gates. Different shades of green depict different amount of qubits. (b) Number of two-qubit gates reduced. Different shades of blue depict different amount of qubits.

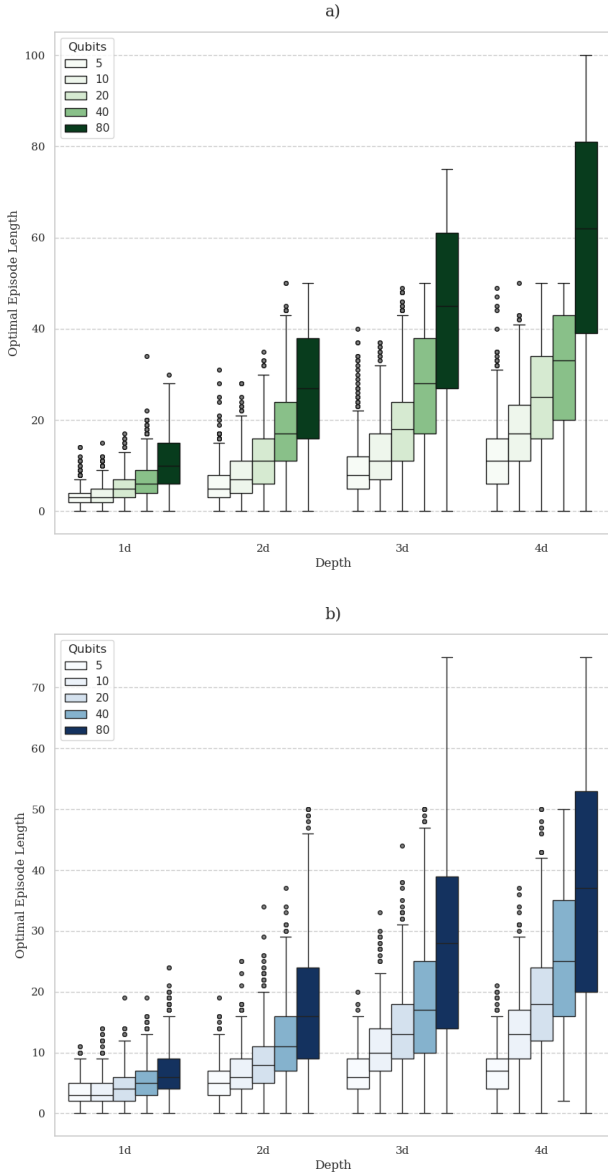


Figure 6: Box plot of the number of actions taken during an episode by the `r1-zx` once trained. Results are drawn from the same tests used to depict the amount of gates reduced. Different shades of green and blue depict different amount of qubits. (a) Actions performed when trying to reduce both single-qubit and two-qubit gates. (b) Actions performed when trying to reduce two-qubit gates.

node features for the critic network using the sum function instead of a global attention layer to capture this extensivity. However, our preliminary tests indicate that, even though results for smaller scale circuits improve, this architecture generalizes worse than our selected one. We leave the exploration on efficient ways of incorporating these features into the network as a future research line. As per the magnitude of improvement, we plot the distribution of the difference in gates between our approach and `cflow-zx`. For the total amount of gates, the agent improves the average compression by a maximum of 150% for 10-qubit circuits of depth twenty, with the improvement decreasing as circuit size grows (except for the outlier behaviour for 5 qubits circuits), maintaining 70% improvement for circuits of 20 qubits and depth 4d and 40 qubits and depth 3d, and reaching a close to 20 – 30% average improvement for the largest studied circuits (Figure 9a). For two-qubit gates, the improvement ranges between 150% and 250%, with a value of 200% for circuits of 80 qubits and depth 4d (eighty) (Figure 9b). All the aforementioned results demonstrate the capacity for the `r1-zx` agent to generalize its learnt strategies to circuits of much larger size, which is crucial to ensure the scalability of the approach.

4.3 Computational Cost

Even though we have seen that our approach is able to outperform its competitors in terms of the quality of the generated circuits, it is important to understand the price to be paid in terms of computational cost to achieve that. In the NISQ era, reducing the amount of gates is not only important to speed up the calculation, but particularly to reduce the probability of errors occurring during the execution. In this sense, the trade-off between the increased execution time of our algorithm and the gain in "quantum computing time" is not one-to-one. Nonetheless, we crudely plot the difference in execution time between the `cflow-zx` algorithm and our approach in Figure 10. We consider the full execution time of the algorithm, until the agent selects the `STOP` action or there are no actions remaining, and not the time required to reach the optimal circuit seen during an episode. We observe that our agent is consistently 10x-15x slower than the `cflow` heuristic, though with a subexponential scaling (at

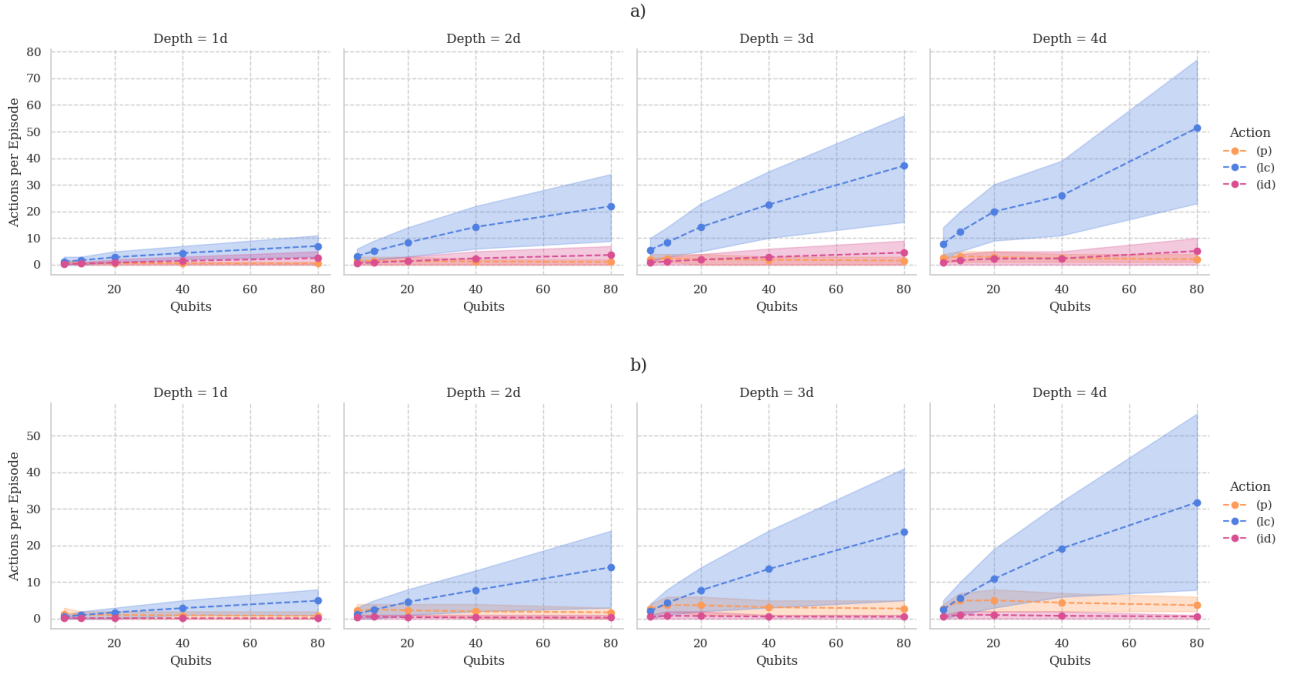


Figure 7: Average number of actions of each type performed per episode by the agent. For clarity, only pivotings (p) (orange), local complementations (lc) (blue), and identity rules (id) (purple) are considered. The non-represented actions are scarcely selected by the agent. Shaded regions represent the interval between percentile 15 and 85 of the distribution. Results are drawn from the same instances. (a) Policy learnt for single-qubit and two-qubit gate reduction. (b) Policy learnt for only two-qubit gate reduction.

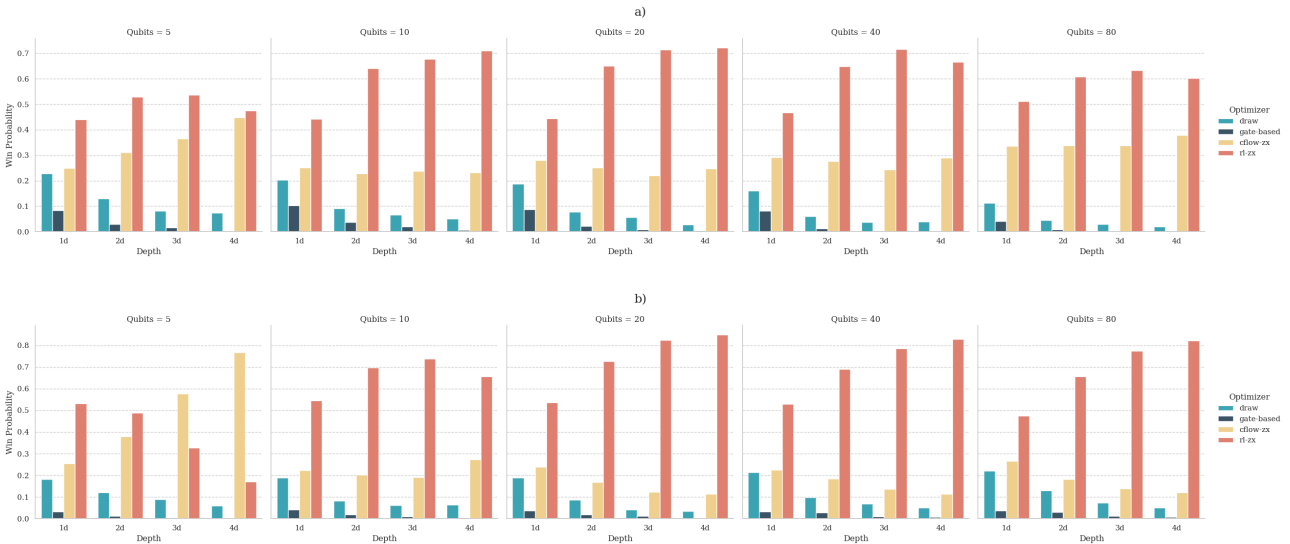


Figure 8: Percentage of test instances for which each optimizer achieves the best compression. Again, results are shown for the same 1000 instances per circuit size and task. Our approach, $r1-zx$, is depicted in orange. 'gate-based' (dark blue) refers to the results after `basic_optimization` and `teleport_reduce` are applied to the initial random circuit, and `cflow-zx` is depicted in yellow. Circuits for which $r1-zx$ ties with either of its competitors are represented as "draw" (light blue). (a) Winning probability per optimizer for single-qubit and two-qubit gate reduction. (b) Winning probability per optimizer for only two-qubit gate reduction.

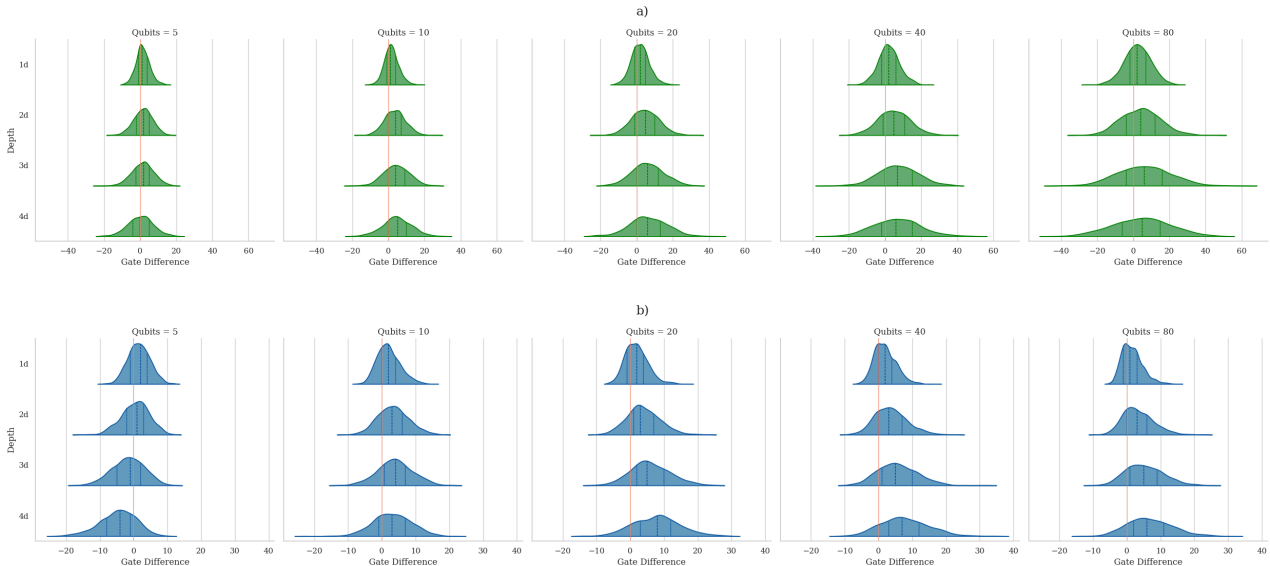


Figure 9: Distribution of the difference in gates between `cflow-zx` and our approach for both optimization tasks and all tested circuit sizes. A positive gate difference implies that `r1-zx` achieves a better compression. Vertical lines, in red, signal a tie between both algorithms. Coloured dashed lines mark the quartiles of the distribution. (a) Single-qubit and two-qubit gate difference, in green. (b) Two-qubit gate difference, in blue.

least for the studied circuits sizes) with both circuit depth and number of qubits. Aside from further research on the agent’s capacity to stop at the optimal time, there are several improvements in terms of the implementation of our solution that can be done to improve on these results. For instance, we have performed naive adaptations of the `PyZX` package to implement the environment, but one could carefully design the action matching procedure (i.e. identifying the actions that are feasible in a diagram) such that it is not applied to the whole graph after each step in an episode, but only on the neighbourhood of the spiders that have been transformed. Additionally, much more sophisticated HPC approaches to parallelize the execution could be explored. In terms of memory, the training on 5 qubit circuits of 60-70 gates requires 2GB of VRAM, for the specific batch size used, and execution of our largest circuits require less than 1 GB.

5 Conclusions & Future work

This work is a continuation of previous exploratory work to develop a novel Reinforcement Learning approach for quantum circuit optimization that exploits the advantages of ZX-Calculus. Here, we improve on our initial methodology by using a more sophisticated scheme based on Graph NNs instead of convolutional layers. To

assess the validity of the method, we present results across three relevant criteria: quality of the optimization, computational efficiency and scalability. These results are benchmarked for Clifford+T circuits against the best-performing ZX-Calculus based circuit optimization algorithm across two differentiated optimization objectives, the total amount of gates in the circuit and two-qubit gates alone. We demonstrate that the agent is able to generalize the learnt strategies and outperform the competition for circuits of up to 80 qubits and 2100 gates for both tasks. This versatility is particularly useful for current experimental platforms, as the reward function can be shaped taking into account the specific properties of the quantum hardware in which the circuit will be executed, e.g., by weighting each type of gate depending on its fidelity, or taking into account qubit coherence times and the depth of the circuit. An unrefined implementation of the agent is only an order of magnitude slower than the `cflow-zx` algorithm optimizing circuits, but with a similar subexponential scaling. A full training process takes around 16 h on a small server.

Notably, we include `teleport_reduce` as a pre-processing step to efficiently deal with T gates in the circuit. A possible extension to our work could be to allow the agent to select the actions applied during this stage as well. Not only that,

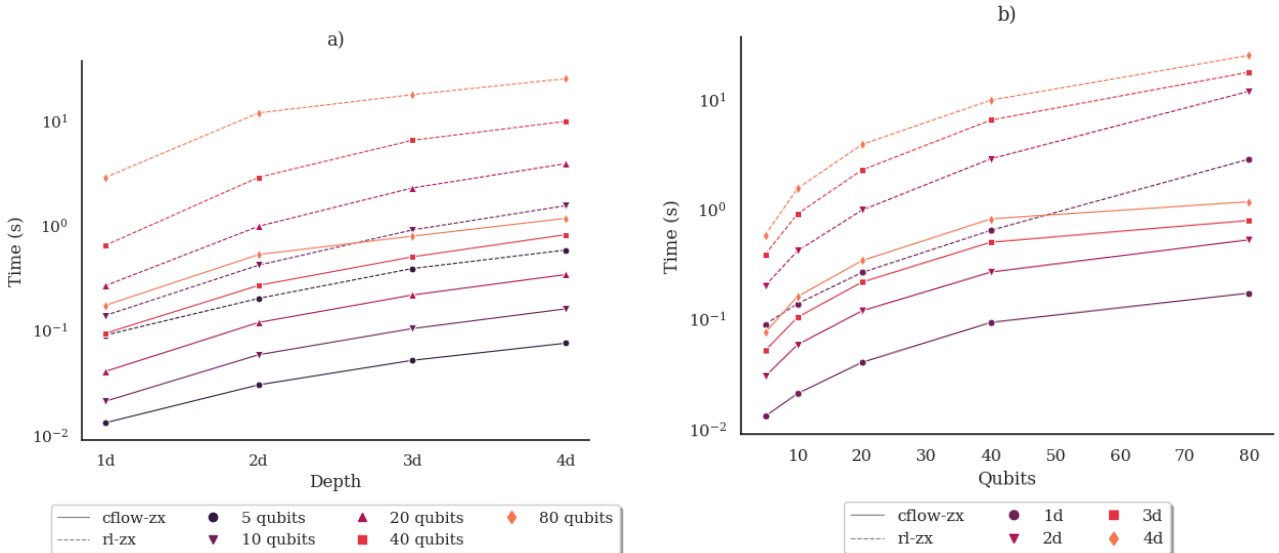


Figure 10: Comparison of the average episode execution time, in seconds, for the cflow-zx algorithm (solid lines) and our approach (dashed lines), with color code dependent on each relevant circuit dimension. (a) Scaling with respect to the average circuit depth. (b) Scaling with respect to the amount of qubits.

the agent is not allowed to use spider unfusion rules as they are not guaranteed to preserve the gflow of the resulting diagram. To allow for these actions to be included, one would then need to ensure the preservation of gflow after each action is applied, which is very computationally expensive. An alternative is to modify our procedure and utilize a simpler extraction process based on cflow preservation, which is less computationally intensive. Additionally, we believe this would facilitate including features in the agent’s observation that inform the agent on the effect of the circuit extraction process for a given diagram, that could both simplify the training phase and improve performance overall. Finally, it is worth noting that further research on the observation features and the overall agent architecture could also improve the agent’s decision on when to stop the optimization, which would greatly benefit the computational performance of the algorithm, as less optimization steps would be required and the circuit extraction process could be used only at the end of the episode. Upon completion of this work, we found reference [34] where the authors use a RL approach for spider-count reduction in ZX-diagrams and reference [35], where circuit optimization is done using Transformers.

6 Data and code availability

Data and code to verify and replicate our results can be found in [36]. Other findings from this study are available from the authors under due request.

Acknowledgments

We thank Professor R.Rey and the Theory&Applications team at Qilimanjaro for their constructive criticism and very helpful advice. A.G-S received funding from the European Union’s Horizon 2020 research and innovation programme under grant agreement No 951911 (AI4Media). This work was supported by the Agència de Gestió d’Ajuts Universitaris i de Recerca through the DI grant (No. 2020-DI00063).

References

- [1] John Preskill. “Quantum computing in the NISQ era and beyond”. *Quantum* **2**, 79 (2018).
- [2] Beatrice Nash, Vlad Gheorghiu, and Michele Mosca. “Quantum circuit optimizations for nisq architectures”. *Quantum Science and Technology* **5**, 025010 (2020).

- [3] Scott Aaronson and Daniel Gottesman. “Improved simulation of stabilizer circuits”. *Phys. Rev. A* **70**, 052328 (2004).
- [4] Vadym Kliuchnikov and Dmitri Maslov. “Optimization of clifford circuits”. *Phys. Rev. A* **88**, 052307 (2013).
- [5] Richard S. Sutton and Andrew G. Barto. “Reinforcement learning: An introduction”. The MIT Press. (2018). Second edition. url: <http://incompleteideas.net/book/the-book-2nd.html>.
- [6] Thomas Fösel, Murphy Yuezhen Niu, Florian Marquardt, and Li Li. “Quantum circuit optimization with deep reinforcement learning” (2021). [arXiv:2103.07585](https://arxiv.org/abs/2103.07585).
- [7] Zikun Li, Jinjun Peng, Yixuan Mei, Sina Lin, Yi Wu, Oded Padon, and Zhihao Jia. “Quarl: A learning-based quantum circuit optimizer” (2023). [arXiv:2307.10120](https://arxiv.org/abs/2307.10120).
- [8] Bob Coecke and Ross Duncan. “Interacting quantum observables: categorical algebra and diagrammatics”. *New Journal of Physics* **13**, 043016 (2011).
- [9] John Schulman, Filip Wolski, Prafulla Dhariwal, Alec Radford, and Oleg Klimov. “Proximal policy optimization algorithms” (2017). [arXiv:1707.06347](https://arxiv.org/abs/1707.06347).
- [10] Jan Nogué. “Reinforcement Learning based Circuit Compilation via ZX-calculus”. Master’s thesis. Universitat de Barcelona. (2023). url: https://diposit.ub.edu/dspace/bitstream/2445/202911/1/Memoria_TFM-JanNogue.pdf.
- [11] Daniel Gottesman. “Theory of fault-tolerant quantum computation”. *Phys. Rev. A* **57**, 127–137 (1998).
- [12] Daniel Gottesman. “The heisenberg representation of quantum computers” (1998). [arXiv:quant-ph/9807006](https://arxiv.org/abs/quant-ph/9807006).
- [13] Aleks Kissinger and John van de Wetering. “PyZX: Large scale automated diagrammatic reasoning”. *Electronic Proceedings in Theoretical Computer Science* **318**, 229–241 (2020).
- [14] Zonghan Wu, Shirui Pan, Fengwen Chen, Guodong Long, Chengqi Zhang, and Philip S. Yu. “A comprehensive survey on graph neural networks”. *IEEE Transactions on Neural Networks and Learning Systems* **32**, 4–24 (2021).
- [15] Bob Coecke and Aleks Kissinger. “Picturing quantum processes: A first course in quantum theory and diagrammatic reasoning”. Cambridge University Press. (2017).
- [16] John van de Wetering. “Zx-calculus for the working quantum computer scientist” (2020). [arXiv:2012.13966](https://arxiv.org/abs/2012.13966).
- [17] Ross Duncan, Aleks Kissinger, Simon Perdrix, and John van de Wetering. “Graph-theoretic simplification of quantum circuits with the ZX-calculus”. *Quantum* **4**, 279 (2020).
- [18] Niel de Beaudrap, Aleks Kissinger, and John van de Wetering. “Circuit extraction for zx-diagrams can be p-hard”. In Schloss Dagstuhl – Leibniz-Zentrum für Informatik. (2022). [arXiv:2202.09194](https://arxiv.org/abs/2202.09194).
- [19] Calum Holker. “Causal flow preserving optimisation of quantum circuits in the zx-calculus” (2024). [arXiv:2312.02793](https://arxiv.org/abs/2312.02793).
- [20] Korbinian Staudacher, Tobias Guggemos, Wolfgang Gehrke, and Sophia Grundner-Culemann. “Reducing 2-qubit gate count for zx-calculus based quantum circuit optimization”. In Quantum Processing and Languages (QPL22). Pages 1–17. (2022). url: <https://elib.dlr.de/188470/>.
- [21] Anton Kotzig. “Eulerian lines in finite 4-valent graphs and their transformations”. In *Colloquium on Graph Theory Tihany 1966* Pages pages 219 – 230 (Academic Press, 1968).
- [22] André Bouchet. “Graphic presentations of isotropic systems”. *J. Comb. Theory Ser. A* **45**, 58–76 (1987).
- [23] Daniel E Browne, Elham Kashefi, Mehdi Mhalla, and Simon Perdrix. “Generalized flow and determinism in measurement-based quantum computation”. *New Journal of Physics* **9**, 250 (2007).
- [24] Robert Raussendorf, Daniel Browne, and Hans Briegel. “The one-way quantum computer—a non-network model of quantum computation”. *Journal of Modern Optics* **49**, 1299–1306 (2002).
- [25] Miriam Backens, Hector Miller-Bakewell, Giovanni de Felice, Leo Lobski, and John van de Wetering. “There and back again: A circuit extraction tale”. *Quantum* **5**, 421 (2021).
- [26] Aleks Kissinger and John van de Wetering. “Reducing the number of non-clifford gates

- in quantum circuits”. *Phys. Rev. A* **102**, 022406 (2020).
- [27] Vincent Danos and Elham Kashefi. “Determinism in the one-way model”. *Phys. Rev. A* **74**, 052310 (2006).
- [28] Mehdi Mhalla and Simon Perdrix. “Finding optimal flows efficiently”. Page 857–868. Springer Berlin Heidelberg. (2008).
- [29] John Schulman, Philipp Moritz, Sergey Levine, Michael Jordan, and Pieter Abbeel. “High-dimensional continuous control using generalized advantage estimation” (2018). [arXiv:1506.02438](https://arxiv.org/abs/1506.02438).
- [30] Petar Veličković, Guillem Cucurull, Arantxa Casanova, Adriana Romero, Pietro Liò, and Yoshua Bengio. “Graph attention networks” (2018). [arXiv:1710.10903](https://arxiv.org/abs/1710.10903).
- [31] Shaked Brody, Uri Alon, and Eran Yahav. “How attentive are graph attention networks?” (2022). [arXiv:2105.14491](https://arxiv.org/abs/2105.14491).
- [32] Adam Paszke, Sam Gross, Francisco Massa, Adam Lerer, James Bradbury, Gregory Chanan, Trevor Killeen, Zeming Lin, Natalia Gimelshein, Luca Antiga, Alban Desmaison, Andreas Köpf, Edward Yang, Zach DeVito, Martin Raison, Alykhan Tejani, Sasank Chilamkurthy, Benoit Steiner, Lu Fang, Junjie Bai, and Soumith Chintala. “Pytorch: An imperative style, high-performance deep learning library” (2019). [arXiv:1912.01703](https://arxiv.org/abs/1912.01703).
- [33] Greg Brockman, Vicki Cheung, Ludwig Pettersson, Jonas Schneider, John Schulman, Jie Tang, and Wojciech Zaremba. “Openai gym” (2016) [arXiv:1606.01540](https://arxiv.org/abs/1606.01540).
- [34] Maximilian Nägele and Florian Marquardt. “Optimizing zx-diagrams with deep reinforcement learning” (2023). [arXiv:2311.18588](https://arxiv.org/abs/2311.18588).
- [35] Francois Charton, Alexandre Krajenbrink, Konstantinos Meichanetzidis, and Richie Yeung. “Teaching small transformers to rewrite ZX diagrams”. In The 3rd Workshop on Mathematical Reasoning and AI at NeurIPS’23. (2023). url: <https://openreview.net/forum?id=btQ7Bt1NLF>.
- [36] Jordi Riu and Jan Nogué. “Code for quantum circuit optimization with rl via zx-calculus”. Github Repository (2023). url: <https://github.com/qilimanjaro-tech/Circopt-RL-ZXCalc>.